



Article

Correlation of Process Conditions, Porosity Levels and Crystallinity in Atmospherically Plasma Sprayed $\text{Yb}_2\text{Si}_2\text{O}_7$ Environmental Barrier Coatings

Robert Vaßen * , Emine Bakan , Doris Sebold and Yoo Jung Sohn

Forschungszentrum Jülich GmbH, Institute of Energy and Climate Research IEK-1, 52425 Jülich, Germany; e.bakan@fz-juelich.de (E.B.); d.sebold@fz-juelich.de (D.S.); y.sohn@fz-juelich.de (Y.J.S.)

* Correspondence: r.vassen@fz-juelich.de

Abstract: Environmental barrier coatings are necessary to protect fibre reinforced ceramics from high recession rates in fast and hot water vapor-containing gases as they typically are found in the hot gas sections of gas turbines. A standard material to protect SiC/SiC composites is atmospherically plasma sprayed (APS) $\text{Yb}_2\text{Si}_2\text{O}_7$. For this material, it is difficult to obtain at reasonable substrate temperatures both low porosity and high crystallinity levels during APS. In this paper results of coatings prepared by a so-called high velocity APS process and also more conventional processes are presented. All coatings have been prepared by a single layer deposition method which avoids inter passage porosity bands. Furthermore, the samples were heat-treated in air at 1300 °C for 100 h and the influence of the topcoat density on the growth of the silica scale on the used silicon bond coat was studied.

Keywords: environmental barrier coatings; thermal spray; ytterbium disilicate



Citation: Vaßen, R.; Bakan, E.; Sebold, D.; Sohn, Y.J. Correlation of Process Conditions, Porosity Levels and Crystallinity in Atmospherically Plasma Sprayed $\text{Yb}_2\text{Si}_2\text{O}_7$ Environmental Barrier Coatings. *J. Compos. Sci.* **2021**, *5*, 198. <https://doi.org/10.3390/jcs5080198>

Academic Editor: Gérard L. Vignoles

Received: 29 June 2021

Accepted: 21 July 2021

Published: 28 July 2021

Publisher's Note: MDPI stays neutral with regard to jurisdictional claims in published maps and institutional affiliations.



Copyright: © 2021 by the authors. Licensee MDPI, Basel, Switzerland. This article is an open access article distributed under the terms and conditions of the Creative Commons Attribution (CC BY) license (<https://creativecommons.org/licenses/by/4.0/>).

1. Introduction

The efficiency of many energy conversion processes, as for example gas turbines, increases with the operation temperature. Therefore, high temperature capable materials have been developed for many years. One attractive class of materials for this application is ceramics as they offer often high temperature capability in combination with high specific strength which is of special importance for aero-engines. On the other hand, monolithic ceramics do not have sufficient toughness and damage tolerance for demanding applications. A breakthrough was the development of long fibre reinforced ceramics, which give largely improved damage tolerance of the materials [1] and so different components have been produced with such ceramic matrix composites (CMCs). A major driving force for this application has been the need for improved materials in the aero-engine sector and the companies have promoted this development over the last decades [2]. An especially interesting CMC material is SiC fibre reinforced SiC. The covalent bond SiC shows extremely low diffusion rates, which result in very good creep properties. SiC forms under an oxidative environment at elevated temperatures a passivation SiO_2 layer, which reduces the further oxidation rate [3]. However, in a gas turbine, the oxidative atmosphere also contains fast flowing water vapor. This water vapor leads to the formation of volatile (oxy) hydroxides, which remove the scale and can lead to massive damage to the whole component [4,5]:



To protect the components, coatings are applied. These layers are called environmental barrier coatings (EBCs). The used materials should first of all have a low recession rate much smaller than the one of silica. Different oxide materials have been investigated by Fritsch et al. [6–8]. In addition to the recession rate also the thermal expansion coefficient

(TEC) plays a major role. The protective coatings have to be gastight and therefore very dense. This is in contrast to thermal barrier coatings, which typically have a high degree of porosity and due to that, a reduced Young's modulus. A low modulus is often beneficial in coating systems as the modulus E_{EBC} determines in combination with the strain given by the mismatch $\alpha_{EBC} - \alpha_{CMC}$ multiplied with the temperature change ΔT the stress state σ_{EBC} in the coatings. For thin coatings, this is given by

$$\sigma_{EBC} = \frac{E_{EBC}(\alpha_{EBC} - \alpha_{CMC})}{1 - \nu_{EBC}} \Delta T \quad (2)$$

where ν_{EBC} is the Poisson's ratio of the EBC [9].

Hence, in EBCs with a high modulus, it is important to use materials with thermal expansion coefficients well adapted to the substrate. It was found that rare earth disilicates have thermal expansion coefficients very similar to one of the SiC/SiC composites. Especially, $\text{Yb}_2\text{Si}_2\text{O}_7$ is frequently used. Although the monosilicate has even lower recession rates than the disilicate, it is not appropriate due to the high thermal expansion coefficient. $\text{Yb}_2\text{Si}_2\text{O}_7$ will also be used in this paper for the EBCs. The dramatic influence of the TEC mismatch will be demonstrated by the additional use of an oxide/oxide substrate with a significantly higher TEC.

EBCs are often applied using atmospheric plasma spraying (APS). In this process, particulate feedstocks are heated and accelerated in a hot, fast gas plume and then deposited on the substrate [10]. During impingement on the substrate, the particles deform and form splats. Furthermore, they cool down from the melting temperature to the substrate temperature, the accompanied shrinkage leads to high tensile stresses in the splats relaxing by the formation of intra and inter splat cracks [11]. This crack network typically allows the penetration of gases. To achieve gas-tight coatings, rather hot and fast spraying conditions with high substrate temperatures (above 500 °C) are beneficial. Such conditions can promote a remelting or at least significant heating of already deposited splats and by this improve the bonding in the coating [12].

In addition, high particle velocities at impact (>300 m/s) are also beneficial [13,14]. So gastight ceramic membranes could be produced by a high temperature and high velocity process at very low pressure plasma spraying [15].

For the often-used silicates, another problem arises during thermal spray. The deposition process with its fast cooling leads often to the formation of amorphous phases. During operation, these phases crystallise, which is accompanied by shrinkage and hence stress and crack formation. As high deposition temperatures are promoting the deposition of the crystalline phase, one possibility is to deposit coatings in a furnace [16,17]. In the approach discussed here, this additional heating is avoided as it is time-consuming and appears difficult for complex components. Instead, specific thermal spray conditions are applied and the influence on both the porosity level and the crystallinity of the coatings is investigated. Although several thermal spray processes are suitable for the deposition of EBCs [18], here, the focus is on atmospheric plasma spraying. Furthermore, it was demonstrated, that the deposition in a single passage improves the density of the coatings as it prevents the formation of porosity bands [19]. This technique is applied in this paper. Additionally, for the APS process, a small nozzle (6 mm) in our TriplexPro torch and high process gas flows (>100 standard litre per minute (slpm)) were used [20]. We call this process high velocity (HV)-APS and the conditions are considered to be beneficial for the manufacture of crystalline and rather dense coatings.

2. Materials and Methods

Before the deposition of the EBC, a Si bond coat was applied using a Si powder (also Oerlikon Metco Inc. Westbury, NY, USA). It was a fused and crushed powder with particle sizes of $d_{10} = 28 \mu\text{m}$, $d_{50} = 40 \mu\text{m}$, and $d_{90} = 59 \mu\text{m}$, where the numbers 10, 50, 90 indicate the percentage of volume fraction below this particle size. For the deposition of the EBCs, an agglomerated sintered monoclinic $\text{Yb}_2\text{Si}_2\text{O}_7$ (YbDS, C2/m, JCPDS No 01-082-0734)

from Oerlikon Metco Inc. Westbury, NY, USA with a mean particle size of $d_{10} = 24 \mu\text{m}$, $d_{50} = 38 \mu\text{m}$, and $d_{90} = 68 \mu\text{m}$ and 5 wt.-% monoclinic Yb_2SiO_5 (YbMS, I2/a, JCPDS No 00-040-0386) was used as impurity phase.

As substrates, two different materials were taken—a fibre-reinforced oxide/oxide CMC called UMOXTM with Nextel 610 Alumina fibres and a matrix produced from sub-micron mullite particles and polysiloxane precursor [21]. In addition, EBC/Si systems were deposited onto roughened α -SiC substrates Saint Gobain Ceramics, Niagara Falls, NY, USA, [22]) with the dimensions of $25 \times 25 \times 5 \text{ mm}^3$. The SiC samples were ultrasonically cleaned before spraying. The mechanical pretreatment was carried out with 80-grit sandpaper or by grit blasting with F 36 SiC powder.

The EBC systems were deposited in a MultiCoat system (Oerlikon Metco, Wohlen, Switzerland), which was operated with the three-cathode TriplexPro 210 mounted on a six-axis robot (IRB 2400, ABB, Zürich, Switzerland).

The silicon bond coat was deposited using 50 slpm Ar, a plasma current of 448 A, and a stand-off distance of 100 mm. The small nozzle with a 6.5 mm diameter was taken [14].

For the EBC deposition, different parameters were applied. Some important spray parameters are given in Table 1. The APS 1 + 2 parameters were similar to the ones given in [23]. However, the parameters were adapted to a meander-type deposition instead of rotating substrates. In addition, feeding rates and gun velocities were changed to manufacture the coatings in a single passage.

Table 1. Mean APS process parameters for the deposition of the topcoat.

Coating Type	Ar (slpm)	He (slpm)	Stand-Off Distance (mm)	Plasma Power (kW)	Nozzle Diameter (mm)
APS1	46	4	90	27.1	9
APS2	46	4	90	37.4	9
HVAPS1	170	4	120	59.6	6.5
HVAPS2	170	8	120	60.2	6.5
HVAPS3	170	4	120	63.7	6.5

For the 3 HVAPS coatings much higher process flows were taken corresponding to the high velocity conditions. Furthermore, feeding rates were increased to realise a single passage deposition.

After spraying the samples were sectioned, polished, and examined with a scanning electron microscope (Ultra 55 Carl Zeiss NTS GmbH, Oberkochen, Germany) combined with an energy-dispersive X-ray INCAEnergy355 spectrometer (EDS, Oxford Instruments Ltd., Abingdon, Oxfordshire, UK). Porosity levels were determined with image analysis using an image thresholding procedure with the ImageJ 1.52i (public domain) using 10–20 SEM images ($\times 1.0 \text{ k}$) to cover minimum $3 \times 10^5 \mu\text{m}^2$ analysis area for each sample. Before and after spraying, the thickness and mass of the samples were determined by a cantilever and a balance.

X-ray diffraction data were collected with an Empyrean facility (Malvern Panalytical, Netherlands) using $\text{Cu-K}\alpha$ -radiation ($\lambda = 1.54187 \text{ \AA}$). The XRD analysis was performed using the TOPAS software (Bruker AXS, Germany). Rietveld analysis was carried out for the quantitative phase analysis (QPA) of crystalline phases and the degree of crystallinity was determined using

$$\text{degree of crystallinity} = 100 \times \frac{\text{crystalline area}}{\text{crystalline area} + \text{amorphous area}} \quad (3)$$

where the crystalline area is the sum of all the integrated Bragg peak intensity of the crystalline phases and the amorphous area is the sum of the integrated intensity of the amorphous hump observed at $2\theta = 30$ and 50° .

All EBC systems were thermally cycled for 100 h at 1300 °C in a furnace in laboratory air. Each 20 h, the samples were taken out of the furnace and cooled down in air to room temperature.

3. Results and Discussion

3.1. As-Sprayed Coatings

In Figure 1 the micrographs of the different coatings are shown in the as-sprayed condition, in Figure 2 after heat treatment (100 h, 1300 °C). As the microstructures of the HV APS coatings do not reveal distinct differences, only HV APS1 is shown.

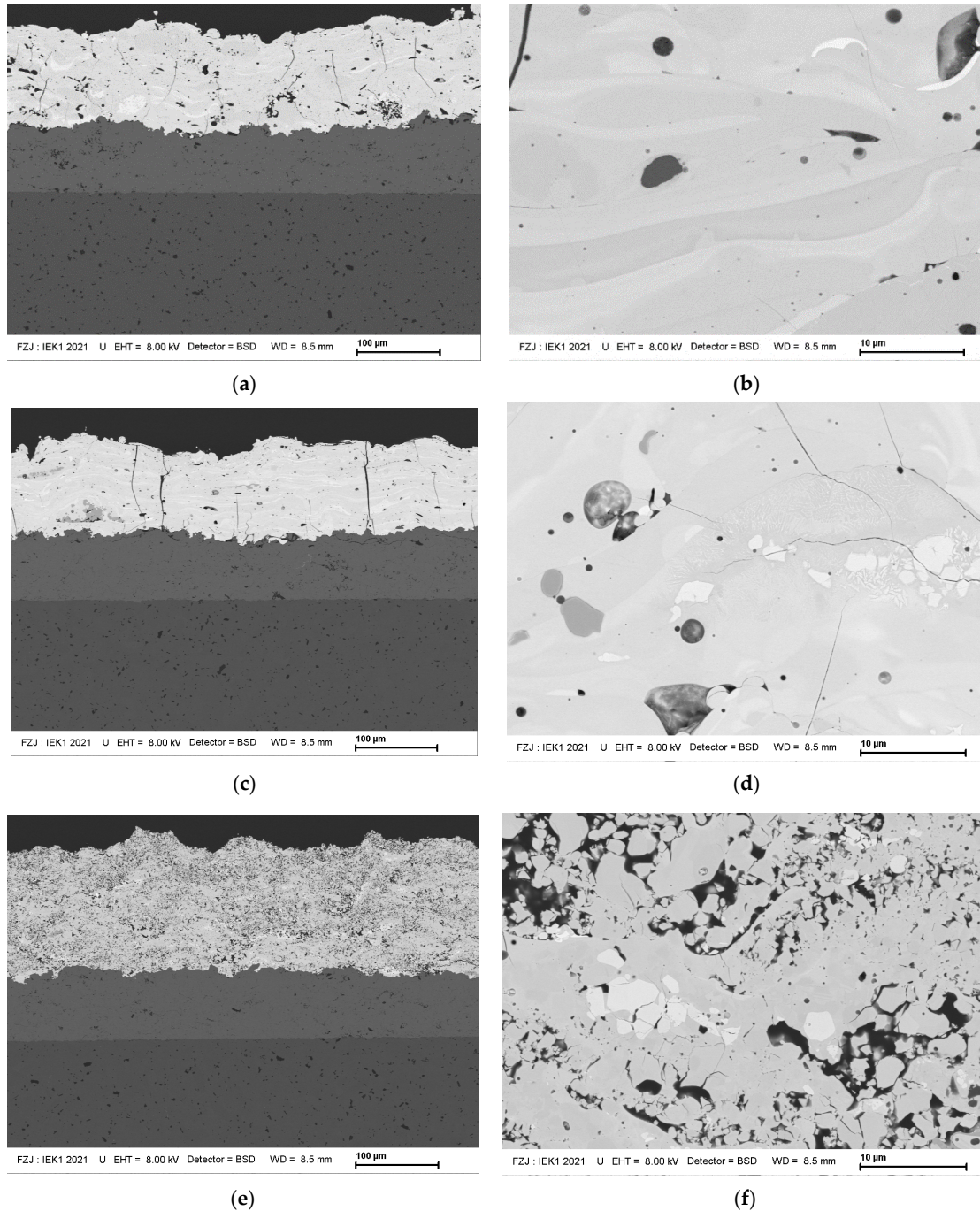


Figure 1. SEM micrographs of as-sprayed YDS coatings, (a,b) APS1, (c,d) APS2, (e,f) HVAPS1.

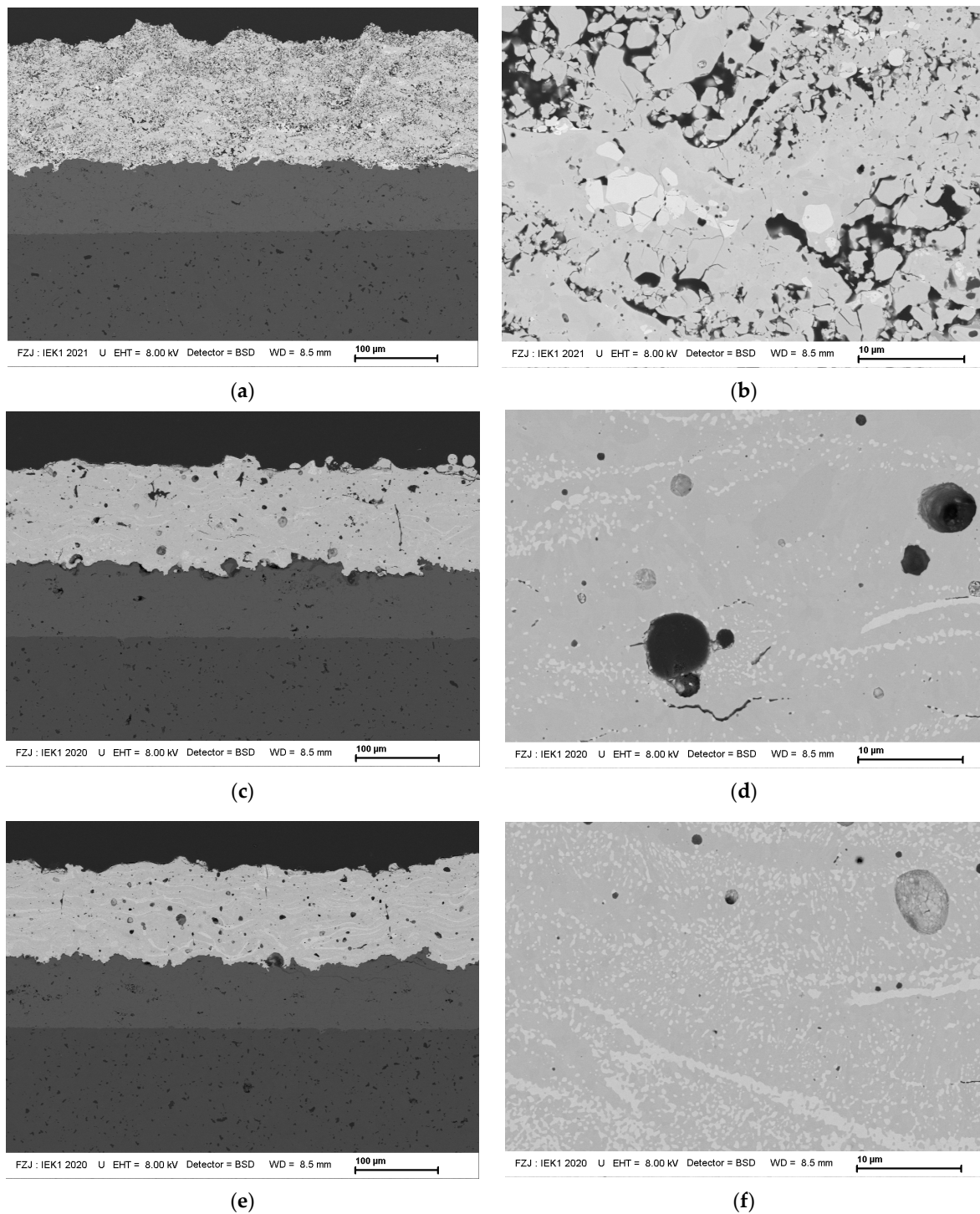


Figure 2. SEM micrographs of the heat-treated YDS coatings (100 h, 1300 °C), (a,b) APS1, (c,d) APS2, (e,f) HV APS1.

In Figures 1 and 2 the micrographs of the different coatings in the as-sprayed condition as well as after heat treatment (100 h, 1300 °C) are shown. The coating thickness of all the different coatings was between 100 and 150 μm. In all images, no signs of inter passage porosity bands are found. These are often formed due to the cooling of the surface between individual passages. Here the used single passage deposition has a clear advantage.

The heat-treated coatings will be discussed in the next chapter. The APS coatings show segmentation cracks and several rather large, spherical pores (Figure 1e,f). The results of image analysis in Figure 3 indicate a lower porosity in the APS2 sample (~4%) than in the APS1 (~7%), which can be explained by the lower plasma power used for the

latter. In addition to the pores and cracks, bright elongated areas exist in the as-sprayed APS coatings, which can be identified as Yb-rich phases. As observed in earlier studies, these areas result from silica loss from the surface of the particles during plasma spraying. Furthermore, some small non-spherical bright areas are found in Figure 1d, which might result from YbMS in the feedstock, and which was probably not completely molten in the APS process, maintaining its faceted appearance.

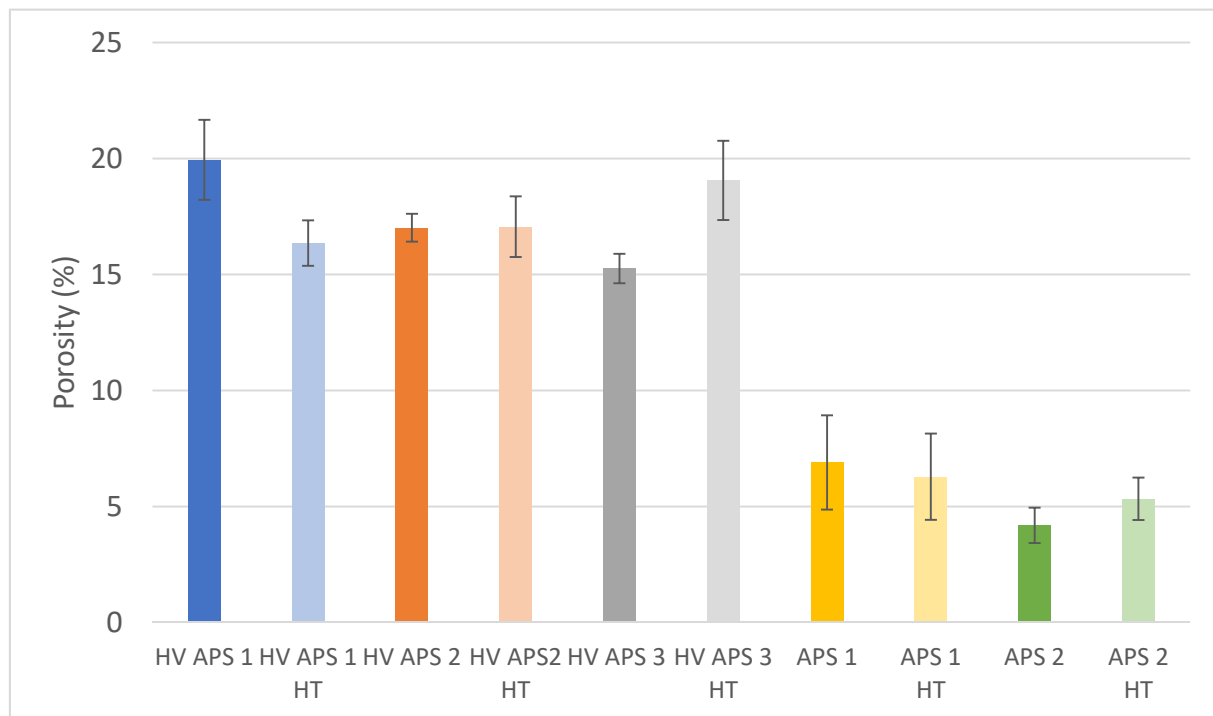


Figure 3. Porosity levels of the different coatings (see Table 1) in the as-sprayed state and after heat treatment (HT, 1300 °C, 100 h).

The microstructure of the HV coatings looks very different. No large cracks can be found in these coatings; however, they contain a rather high amount of porosity (Figure 1e,f). The porosity in the as-sprayed condition decreases from HV-APS1 to HV APS2, which can be a result of the higher amount of Helium used, which increases the temperature and heat transfer of the plasma gases. Even a higher reduction is possible by the increase of the power (HV APS3). The microstructure (Figure 1f) does not show the bright elongated areas as found in the conventional APS coatings (Figure 1b,d). Instead, only the bright faceted areas are found, which are probably remaining from the YbMS phase in the feedstock powder. These results are a clear indication that only a minor loss of silica takes place during deposition, which is an obvious advantage as it avoids impurity phase formation.

As the efficiency of the process is a good indication of the degree of molten state in an atmospheric plasma spraying process, this will also be analysed (Figure 4). In this investigation, the efficiency has been calculated in two different ways, first from the mass gain and second from the thickness. For the evaluation from the thickness, it was assumed that the deposited layers are porous with porosity levels given in Figure 3. Especially the values of the APS coatings are very high, the slightly higher values than 1 are attributed to experimental error.

Both efficiency results are plotted in Figure 4 as a function of the power normalised to the total gas flow. Although the absolute power was the highest for the runs HVAPS1-3, the specific power is due to the large gas flows lower than for the other two conditions. This leads to reduced efficiency of 30 to 40% compared to values of 70 to 100% for the conventional APS (efficiency from mass gain), and, as discussed later, also to a higher

porosity level. The reduced specific power means that the energy content per atom and hence the temperature is reduced in the gas. This leads to reduced energy transfer to the particles and reduced heating. In addition, the smaller nozzle of the HV process combined with the high gas flows lead to increased velocities of the plasma gas and, from that, to reduced time to heat the particles in the plasma plume. On the other hand, the higher gas velocities will lead to increased velocities of the particles and that should reduce the porosity levels. However, this effect was not dominating here as the porosity levels remained quite high. In Figure 5, the degree of crystallinity as a function of the normalised power is plotted. Here it is amazing that for the HVAPS coatings nearly 100% crystallinity results compared to 15 to 50% for the conventional APS. The high velocity APS results in very high gas and particle velocities while keeping the temperatures of the plasma moderate. This will lead to no melting or only melting of the surface of the particles in the plasma plume. Hence, the major central part of the particle remains solid and will maintain its crystallinity during spraying. In addition, also the remaining crystals might serve as nucleation sites for crystallisation even during the fast cooling process. The high velocity and hence high kinetic energy should in the HV process be able to allow the deformation of the solid centre of the particles and thereby the formation of a rather dense coating. In our tests, the used HV APS conditions were extreme towards maintaining the crystallinity. Modified process conditions with a specific power between 0.4 and 0.5 kW/slp_m will be investigated in the near future.

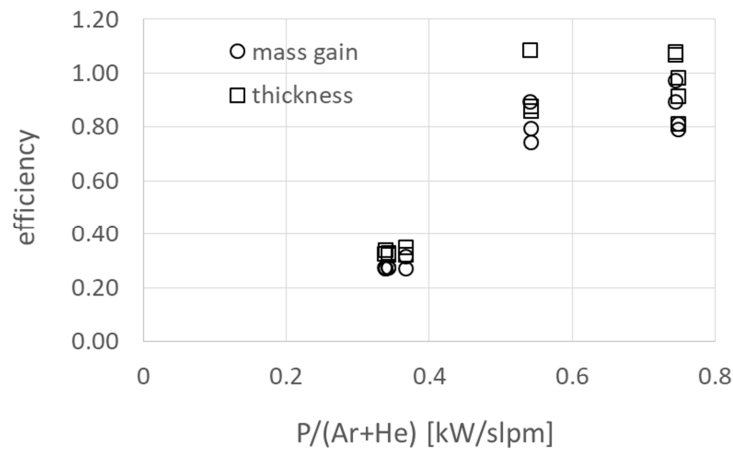


Figure 4. Efficiency of the different spray trials as a function of the power normalised to the total gas flow (circles: efficiency from mass gain, squares: from coating thickness) for different substrates.

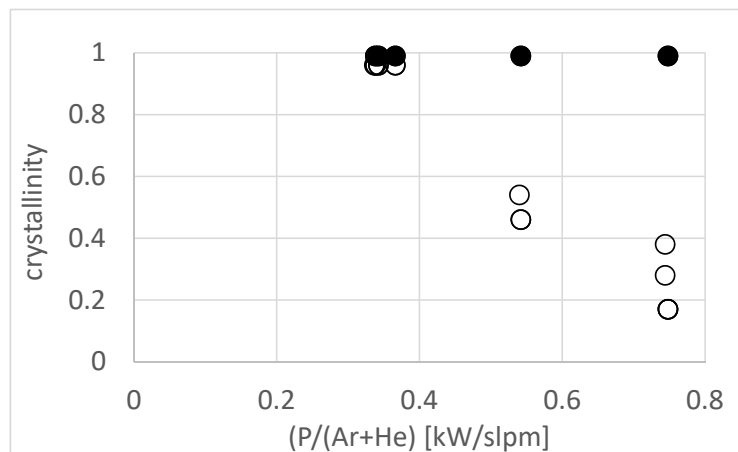


Figure 5. Degree of crystallinity of the as-sprayed (open symbols) and heat-treated (100 h, 1300 °C, closed symbols) coatings as a function of the power normalised to the total gas flow for different substrates.

The high degree of crystallinity is a unique result, showing clearly the potential of the new deposition conditions. The possibility to maintain the phase composition of the feedstock powder prevents the process of crystallisation during subsequent heat treatment, which is accompanied by volume changes and can introduce stresses and cracks.

In addition to the high degree of crystallinity, the formed crystalline phases were also analysed. In Figure 6, the results of the Rietveld refinements are presented. The major phase in all coatings is the β -Ytterbium disilicate (YbDS, 01-082-0734) the minor phase is X2-Ytterbium monosilicate phase (YbMS, 00-040-0386), which appears due to silica loss or as already present in the feedstock. No other phases were found in contrast to other publications [24], neither in the as-sprayed state nor after heat treatment.

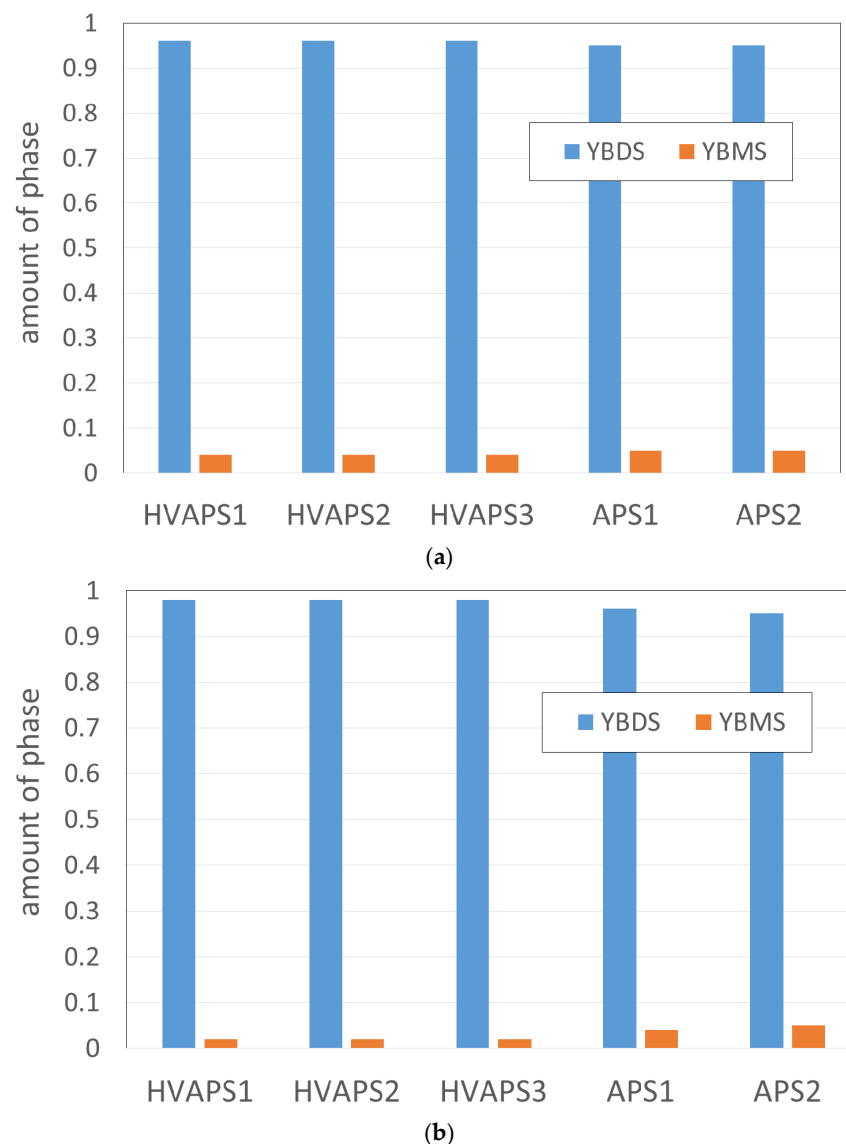


Figure 6. Amount of crystalline $\text{Yb}_2\text{Si}_2\text{O}_7$ (YbDS) and Yb_2SiO_5 (YbMS) phases in the as-sprayed coatings (a) and after heat-treatment at 1300 °C for 100 h (b).

In the as-sprayed condition, about 4 wt.-% YbMS is found for the HV conditions (with about 95% crystallinity) and 5 wt.-% YbMS for the conventional APS conditions (50 wt.-% or less crystallinity). As discussed in the next chapter, the differences are more pronounced after the heat treatment (Figure 6b).

3.2. Coatings after Heat Treatment

At first, the impact of the cycles between RT and 1300 °C (in total 5×20 h cycles) is described. As outlined before, for the cycling both oxide/oxide CMCs and SiC substrates have been used. Due to the high alumina fibre content (~50 vol.-%), the mean thermal expansion coefficient of the CMC between RT and 1300 °C is about $7 \times 10^{-6}/\text{K}$, while that of sintered SiC is between RT and 700 °C about $4 \times 10^{-6}/\text{K}$ [22]. The TEC of YbDS from RT to 1300 °C is about $4 \times 10^{-6}/\text{K}$ [25], generating low stress levels on the SiC substrates during cycling, and rather high values for the CMC substrate. Using the Young's modulus of dense sintered YbDS (168 GPa), the Poisson's ratio of 0.3 ([25]) and assuming full relaxation at elevated temperature, a tensile stress of about 918 MPa can be calculated after cooling for oxide/oxide CMCs (Equation (2)). This high stress level is too high to be tolerable for thick coatings due to the high elastically stored energy G . A value of G in the order of $376 \text{ J}/\text{m}^2$ results for a $150 \mu\text{m}$ layer [26]. This value is higher than the ones of well-bonded thermal barrier coatings ($150 \text{ J}/\text{m}^2$, [27]) and hence, all coatings on the CMC substrates spalled off at the end of the first cycle, even those with lower Young's modulus present in the HV APS samples. At the beginning of the cooling process, the coatings were still intact as visible in Figure 7.

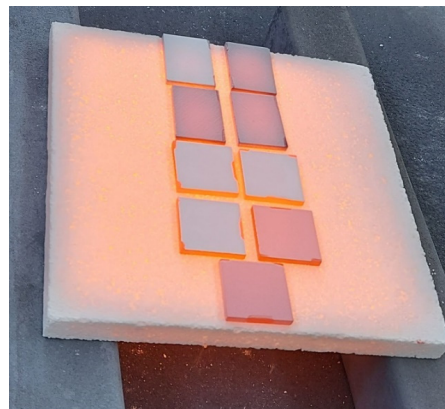


Figure 7. Different samples after beginning of the cooling down from the first cycle (1300 °C, 20 h), left to right and top to bottom the samples are HVAPS1, APS1, APS2*, APS2, HVAPS1, HVAPS2, HVAPS3, APS1, APS2. * indicates slightly reduced feeding rate.

In contrast to the EBCs on the oxide CMC substrates, the EBC on SiC substrates did not show any sign of delamination or crack formation after thermal cycling indicating the excellent thermal cyclic performance of these coating systems.

It is interesting to note that the APS samples appeared dark in contrast to the HVAPS sample being white (Figure 7). This can be related to the higher number of fine pores in the HVAPS coatings which scatter visible light efficiently.

The microstructure of the heat-treated samples (Figure 2) can be compared to the as-sprayed coating in Figure 1. Interestingly, the cracks in the APS coatings disappeared nearly completely without further damage to the coatings. The crystallisation of the silicate phase took place during the heat treatment (see Figure 5) and that should result in shrinkage and stress build-up. A crystallinity of 30 to 50 wt.-% (see Figure 5) leads to a reduced shrinkage which can be tolerated under the present, rather moderate cyclic conditions without cracking. In [28] the shrinkage during crystallisation was partly compensated by a phase transformation of a metastable monosilicate. This seems to have no relevance in the present investigation as even for the APS coatings the silica loss has to be rather limited as the amount of YbMS (4–5 wt.-%, see Figure 6) is similar to the amount in the feedstock. Some YbMS is present in the coatings, which resulted in a precipitation of the YbMS phase. These can be seen as bright dots in Figure 1d,h. This was also found earlier in annealed plasma-sprayed YbDS [28]. Major silicon loss or also the direct use of YbMS as coating

material can certainly involve cracking of the coating due to the larger thermal expansion coefficient compared to the substrate [16].

Although the cracks were completely closed during sintering, the total porosity (Figure 3) remained rather unchanged. A possible explanation can be that the sintering process is dominated by surface diffusion. Then the sintering only leads to coarsening of the pores/cracks without densification and hence pore volume reduction. Pores with a large surface area as cracks will turn into spherical pores as the sphere has the lowest surface of any geometrical body. Furthermore, especially in the APS2 coating with a lower degree of crystallinity, the heat treatment leads to crystallisation and pore formation, which corresponds to the porosity increase in this sample after heat treatment.

Looking at the effect of the heat treatment on the phase evolution (Figure 6), it is obvious that the amount of YbMS is reduced in the HVAPS samples compared to the APS samples. Although the silicon loss and hence the formation of monosilicate is limited under the used APS conditions, it is negligible for the HVAPS conditions, especially if one has in mind that the starting powder already contained some amount of monosilicate.

After the thermal cycling, the thickness of the silica scale formed on the silicon bond coat was also measured (see Figure 8). This thermally grown oxide is typically formed in EBC systems during operation and is considered to play a major role in the delamination of the coatings [29]. The thickness under the more porous HVAPS coatings is higher than under the APS coatings. The thickness of the silica scale under the porous HVAPS coatings is close to the extrapolated results of the parabolic thin film oxidation of single crystal silicon, which gives a thickness of about 1.7 μm [30]. In contrast to the assumption of parabolic oxidation kinetics, in [28], linear oxidation behaviour of silicon bond coats underneath a YbDS coating was found. This was attributed to oxygen diffusion through the YbDS layer being the rate-determining step. As this thickness is constant, a linear oxidation kinetic follows. In the present investigation, we did not compare different oxidation times and hence, we cannot directly conclude on the kinetics. However, it is possible to compare the observed scale thickness. In [28] a gas flow of 90% $\text{H}_2\text{O}/10\% \text{O}_2$ was used giving an oxygen partial pressure of 0.1 bar. As discussed in this paper, the scale growth rate should be directly proportional to the oxygen partial pressure and inversely proportional to the YbDS layer thickness. The thickness in our investigation is similar (100 μm) while the oxygen partial pressure is higher (air, 22%). Hence, we obtained a corresponding scale thickness of about 400 nm (see Figure 8). This fits excellently to the values supplied in [28], although one has to state that there a slightly higher temperature (1316 $^\circ\text{C}$) was used. If one determines the time when both scale thicknesses are equal (linear and square root), a time of about 15,000 h results. Hence, this would explain why in [28] no deviation from the linear law was observed till the 2000 h measurement time.

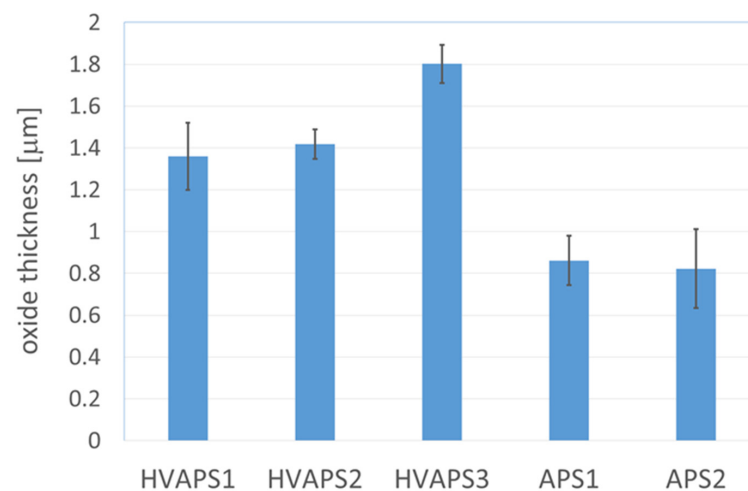


Figure 8. Thickness of the oxide layer after 5×20 h cycles at 1300 $^\circ\text{C}$ for the different coatings.

4. Conclusions

In this paper $\text{Yb}_2\text{Si}_2\text{O}_7$ environmental barrier coatings on silicon bond coats have been produced by an atmospheric plasma spraying process using single layer deposition. Coatings prepared by High Velocity APS showed an excellent degree of crystallinity (>95%) in the as-sprayed state, however, porosity levels are still about 15% high and have to be further reduced. In contrast, APS coatings revealed lower crystallinity (30–50%) and low porosity (4–7%).

During thermal cycling (5×20 h cycles at 1300°C), coatings on oxide/oxide CMCs spalled off at the end of the first cycle due to the large thermal expansion mismatch between coating and substrate. In contrast, coatings on SiC substrates survived without any spallation or crack formation. These coatings could reduce the oxidation rates of the silicon bond coat revealing a gas tightness similar to coatings sprayed in a furnace.

Author Contributions: Conceptualization, R.V.; Formal analysis, E.B., D.S. and Y.J.S.; Investigation, R.V. All authors have read and agreed to the published version of the manuscript.

Funding: This research received no external funding.

Institutional Review Board Statement: Not applicable.

Informed Consent Statement: Not applicable.

Data Availability Statement: The data presented in this study are available on request from the corresponding author.

Acknowledgments: The authors would like to acknowledge the support of Markus Wolf, Daniel Mack, and Georg Mauer in the HV-APS development. The authors also thank Frank Kurze for performing the thermal spray experiments.

Conflicts of Interest: The authors declare no conflict of interest.

References

1. Bansal, N.P. (Ed.) *Handbook of Ceramic Composites*; Kluwer: Boston, MA, USA, 2005.
2. Steibel, J. Ceramic matrix composites taking flight at GE Aviation. *Am. Ceram. Soc. Bull.* **2019**, *98*, 30–33.
3. Roy, J.; Chandra, S.; Das, S.; Maitra, S. Oxidation behaviour of silicon carbide—A review. *Rev. Adv. Mater. Sci.* **2014**, *38*, 29–39.
4. Opila, E.J.; Hann, R.E. Paralineer Oxidation of CVD SiC in Water Vapor. *J. Am. Ceram. Soc.* **1997**, *80*, 197–205. [[CrossRef](#)]
5. Herrmann, M.; Klemm, H. *Corrosion of Ceramic Materials*; Sarin, V.K., Ed.; Comprehensive Hard Materials; Elsevier: Oxford, UK, 2014.
6. Fritsch, M.; Klemm, H.; Herrmann, M.; Michaelis, A.; Schenk, B. The water vapour hot gas corrosion of ceramic materials. *Ceram. Forum Int.* **2010**, *87*, 11–12.
7. Fritsch, M.; Klemm, H.; Herrmann, M.; Schenk, B. Corrosion of selected ceramic materials in hot gas environment. *J. Eur. Ceram. Soc.* **2006**, *26*, 3557–3565. [[CrossRef](#)]
8. Fritsch, M. *Heißgaskorrosion Keramischer Werkstoffe in H_2O -Haltigen Rauchgasatmosphären*; Kompetenzen in Keramik Fraunhofer IRB Verlag: Dresden, TU, USA, 2007.
9. Begley, M.R.; Hutchinson, J.W. *The Mechanics and Reliability of Films, Multilayers and Coatings*; Cambridge University Press: Cambridge, UK, 2017.
10. Pfauchais Pierre, L.; Herberlein Joachim, V.R.; Boulos, M.I. *Thermal Spray Fundamentals*; Springer: New York, NY, USA, 2014.
11. Mutter, M.; Mauer, G.; Mücke, R.; Guillon, O.; Vaßen, R. Correlation of splat morphologies with porosity and residual stress in plasma-sprayed YSZ coatings. *Surf. Coat. Technol.* **2017**, *318*, 157–169. [[CrossRef](#)]
12. Guo, H.B.; Vaßen, R.; Stöver, D. Atmospheric plasma sprayed thick thermal barrier coatings with high segmentation crack density. *Surf. Coat. Technol.* **2004**, *186*, 353–363. [[CrossRef](#)]
13. Vaßen, R.; Stöver, D. Development of thin and gastight ceramic coatings by atmospheric plasma-spraying. In Proceedings of the 2006 International Thermal Spray Conference, Seattle, WA, USA, 15–18 May 2006; Marple, B.R., Hyland, M.M., Lau, Y.-C., Lima, R.S., Voyer, J., Eds.; ASM International: Materials Park, OH, USA, 2006.
14. Bakan, E.; Mauer, G.; Sohn, Y.J.; Koch, D.; Vaßen, R. Application of High-Velocity Oxygen-Fuel (HVOF) Spraying to Fabrication of $\text{Yb}_2\text{Si}_2\text{O}_7$ Environmental Barrier Coatings. *Coatings* **2017**, *7*, 55. [[CrossRef](#)]
15. Marcano, D.; Ivanova, M.E.; Mauer, G.; Sohn, Y.J.; Schwedt, A.; Bram, M.; Menzler, N.H.; Vaßen, R. PS-PVD Processing of Single-Phase Lanthanum Tungstate Layers for Hydrogen-Related Applications. *J. Therm. Spray Technol.* **2019**, *28*, 1554–1564. [[CrossRef](#)]
16. Richards, B.T.; Wadley, H.N.G. Plasma spray deposition of tri-layer environmental barrier coatings. *J. Eur. Ceram. Soc.* **2014**, *34*, 3069–3083. [[CrossRef](#)]

17. Richards, B.T.; Zhao, H.; Wadley, H.N.G. Structure, composition, and defect control during plasma spray deposition of ytterbium silicate coatings. *J. Mater. Sci.* **2015**, *50*, 7939–7957. [[CrossRef](#)]
18. Bakan, E.; Marcano, D.; Zhou, D.; Sohn, Y.J.; Mauer, G.; Vaßen, R. Yb₂Si₂O₇ Environmental Barrier Coatings Deposited by Various Thermal Spray Techniques: A Preliminary Comparative Study. *J. Therm. Spray Technol.* **2017**, *26*, 1011–1024. [[CrossRef](#)]
19. Vassen, R.; Hathiramani, D.; Stöver, D. Verfahren zur Herstellung Dünner, Dichter Keramischichten. EP 1,789,600,81, 4 August 2005.
20. Mauer, G.; Sebold, D.; Vaßen, R.; Hejrani, E.; Naumenko, D.; Quadackers, W.J. Impact of Processing Conditions and Feedstock Characteristics on Thermally Sprayed MCrAlY Bondcoat Properties. *Surf. Coat. Technol.* **2017**, *318*, 114–121. [[CrossRef](#)]
21. Gerenda's, M.S.; Cadoret, Y.; Wilhelmi, C.; Machry, T.; Knoche, R.; Behrendt, T.; Aumeier, T.; Denis, S.; Koch, D.; Tushtev, K.; et al. Improvement of Oxide/Oxide CMC and Development of Combustor and Turbine Components in the Hipoc Program. In Proceedings of the ASME Turbo Expo 2011, New York, NY, USA, 12 October 2010.
22. Hexoloy®SA Silicon Carbide. Available online: https://www.ceramicsrefractories.saint-gobain.com/sites/imdf.hpr.com/files/hexoloy-sa-sic-tds_0.pdf (accessed on 26 July 2021).
23. Bakan, E.; Sohn, Y.J.; Kunz, W.; Klemm, H.; Vaßen, R. Effect of processing on high-velocity water vapor recession behavior of Yb-silicate environmental barrier coatings. *J. Eur. Ceram. Soc.* **2019**, *39*, 1507–1513. [[CrossRef](#)]
24. Garcia, E.; Lee, H.; Sampath, S. Phase and microstructure evolution in plasma sprayed Yb₂Si₂O₇ coatings. *J. Eur. Ceram. Soc.* **2019**, *39*, 1477–1486. [[CrossRef](#)]
25. Zhou, Y.C.; Zhao, C.; Wang, F.; Sun, Y.J.; Zheng, L.Y.; Wang, X.H. Theoretical Prediction and Experimental Investigation on the Thermal and Mechanical Properties of Bulk beta-Yb₂Si₂O₇. *J. Am. Ceram. Soc.* **2013**, *96*, 3891–3900. [[CrossRef](#)]
26. Vaßen, R.; Bakan, E.; Gatzen, C.; Kim, S.; Mack, D.E.; Guillon, O. Environmental Barrier Coatings Made by Different Thermal Spray Technologies. *Coatings* **2019**, *9*, 784. [[CrossRef](#)]
27. Vaßen, R.; Bakan, E.; Mack, D.; Schwartz-Lückge, S.; Sebold, D.; Sohn, Y.J.; Zhou, D.P.; Guillon, O. Performance of YSZ and Gd₂Zr₂O₇/YSZ double layer thermal barrier coatings in burner rig tests. *J. Eur. Ceram. Soc.* **2020**, *40*, 480–490. [[CrossRef](#)]
28. Richards, B.T.; Young, K.A.; De Francqueville, F.; Sehr, S.; Begley, M.R.; Wadley, H.N. Response of ytterbium disilicate–silicon environmental barrier coatings to thermal cycling in water vapor. *Acta Mater.* **2016**, *106*, 1–14. [[CrossRef](#)]
29. Sullivan, R.M. On the oxidation of the silicon bond coat in environmental barrier coatings. *J. Eur. Ceram. Soc.* **2021**, *41*, 557–562. [[CrossRef](#)]
30. Lassig, S.E.; Crowley, J.L. The Kinetics of Low-Pressure Rapid Thermal Oxidation of Silicon. Rapid Thermal Annealing/Chemical Vapor Deposition and Integrated Processing Pittsburgh. *Mater. Res. Soc.* **1989**, *146*, 307–312. [[CrossRef](#)]